

Tomographic characterization of gas jets for Laser-plasma acceleration with increased sensitivity

Uddhab Chaulagain^{*a}, Stefan Karatodorov^a, Marek Raclavský^{a,b}, S. Lorenz^{a,b}, Marcel Lamač^{a,c}, Martin Albrecht^{a,b}, Vidmantas Tomkus^d, Juozas Dudutis^d, Miglė Mackevičiūtė^d, Paulius Gečys^d, and Jaroslav Nejdla^a

^aELI Beamlines, Institute of Physics ASCR, Na Slovance 2, 182 21 Prague 8, Czech Republic;

^bCzech Technical University in Prague, Prague 166 36, Czech Republic;

^cFMP Charles University, Ke Karlovu 3, 12116 Prague 2, Czech Republic;

^dCenter for Physical Sciences and Technology, Savanoriu Ave. 231, LT-02300, Vilnius, Lithuania

*uddhab.chaulagain@eli-beams.eu; phone +420 266 051 455; www.eli-beams.eu

ABSTRACT

We present a new interferometric technique for gas jets density characterization employing a Wollaston shearing interferometer. The distinctive feature of this setup is the double pass of the probe beam through the gas target facilitated by a relay-imaging object arm that images the object on itself and preserves the spatial information. The double pass results in two-fold increase of sensitivity at the same time as the relay-imaging enables the characterization of gas jets with arbitrary gas density distribution by tomographic reconstruction. The capabilities of the double-pass Wollaston interferometer are demonstrated by tomographic density reconstruction of rotationally non-symmetric gas jets that are used as gas targets for the betatron X-ray source at ELI-Beamlines.

Keywords: Gas jet density characterization, interferometry, Wollaston shearing interferometer, tomographic reconstruction, laser-plasma wakefield acceleration, betatron x-ray source.

1. INTRODUCTION

One of the most promising implementations of the laser-plasma accelerator (LPA) [1] is a betatron X-ray source, a compact synchrotron source of femtosecond X-ray pulses with a high brightness [2]. This broadband source of hard X-ray radiation is produced when a femtosecond laser with an intensity above 10^{18} W/cm² collides with a gas medium. It is characterized by a very short pulse duration (\sim fs), a small source size (\sim μ m), and a very high peak brightness. With these unique properties, the betatron source is an integral part of several high-power laser facilities around the world [3]- [8] for applications ranging from high-resolution radiography [9]-[10], to time-resolved measurements of a dynamical shock wave in a matter [11] and warm dense matter (WDM) [12]. The LPA uses supersonic gas jets (He, He/N₂, dry air, or gas clusters [13]-[16]) as targets for the generation of accelerated electron bunches. These gas jet targets routinely employ complex gas density distributions (e.g. tailored gas density [17]), enabling both the optimization of the electron acceleration and the X-ray generation from the accelerated electron bunches. The rapid advances of laser technology led to a gradual increase in laser pulse energies resulting in a decrease in gas jet dimensions or gas jet densities due to the X-ray generation scaling laws [18]. These trends make gas jet density characterization crucial for the optimization of the betatron source. Even more so, as the accumulated probe beam phase shift can be comparable to the sensitivity limit of the measurement methods, especially for low refractive index gases like He. This is the driving force for sensitivity improvement of conventional interferometric methods and the development of new gas characterization techniques.

Here, we present a new interferometric setup for high sensitivity optical probing – double-pass relay-imaging shearing interferometer with a Wollaston prism for gas density characterization of LPA targets. The distinctive characteristic of this interferometer is the double pass of the probe beam through the weakly refracting object (gas jet) facilitated by the relay-imaging object arm. The double pass of the probe through the investigated object enables a two-fold increase of the accumulated phase and improvement of the sensitivity. The relay-imaging arm allows for studying gas jets with complex (arbitrary) gas density distributions by multiple projections and tomographic reconstruction. The improved sensitivity of the double-pass optical configuration is demonstrated by comparing it to the standard single-pass configuration for characterization of both rotationally symmetric gas jets produced by a cylindrical nozzle and non-rotationally symmetric

elongated gas jets produced by a slit nozzle. We performed high-sensitivity tomographic characterization of the slit nozzle with complex gas density spatial distribution and validated the interferometric results by 3D fluid gas density simulations.

2. DOUBLE PASS SHEARING INTERFEROMETRY SYSTEM

The experimental setup presented here is employing double-pass optical probing configuration and a shearing interferometer with a Wollaston prism. The distinctive characteristic of this setup is the double-pass of the probe beam through the low-refractive object – gas jet, which is facilitated by a relay-imaging object arm that is built using only passive optical elements. In addition, the relay-imaging object arm is capable of preserving the spatial information of the object undistorted which allows the use of the double-pass setup for characterization of complex gas distribution through multiple projections of the object from different angles and tomographic reconstruction algorithms. Besides, the relay-imaging object arm is capable of preserving the spatial information of the object undistorted, which allows the use of the double-pass setup for characterization of complex gas distribution through multiple projections of the object at different angles and tomographic reconstruction algorithms.

2.1 Setup of the double-pass shearing Wollaston interferometer

A sketch of the setup of the double-pass Wollaston prism interferometer with relay-imaging is shown in Figure 1. The optical source, a 405 nm monomode fiber laser, collimated by a singlet lens to a 20 mm laser beam diameter, enters the interferometer setup from the left. Due to the shorter wavelength of the laser compared to the conventionally used He-Ne laser (632.8 nm), a higher phase sensitivity is obtained due to larger wavenumber and higher refractive index of the Ar gas [19].

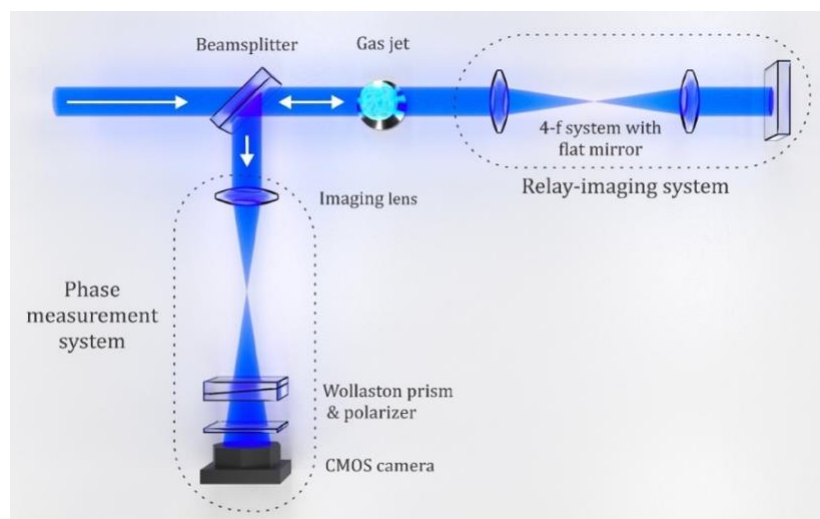


Figure 1. Schematic setup of the double-pass shearing Wollaston interferometer with object relay imaging used for density characterization of gas jets.

The collimated laser beam is partially transmitted through a 50/50 beamsplitter and travels to the weakly refracting gas jet, placed in a vacuum chamber. After the gas jet, the beam travels to the relay-imaging optical system that consists of a 4-f telescope configuration of two doublet achromatic lenses (with 50 cm focal length) and a plane mirror. The relay-imaging system facilitates both the second pass of the collimated probing beam through the gas jet and, at the same time, preserving the spatial information in the beam undistorted by propagation. After the second pass through the gas jet, the laser beam is partially reflected by the beamsplitter and directed to the phase measurement system. This system consists of an imaging lens (with 30 cm focal length), a Wollaston prism (1-degree deviation angle), a polarizer, and a CMOS camera. Due to the characteristics of shearing interferometry with a Wollaston prism, a reference beam is not required for this setup, as the prism splits the incoming beam into two outgoing beams with different polarizations. The interference of these two beams after passing through the polarizer is detected on the camera.

For the comparison of the double-pass setup to the standard single-pass configuration, two turning mirrors are inserted in the optical setup – one after the gas jet and one before the phase measurement system. In this way, the laser beam is sent to the phase measurement system after only a single pass through the object.

With the presented interferometer setup with Wollaston prism, we can acquire individual interferograms of low-pressure gas jets, extract from them the phase accumulated by the probe beam and reconstruct the gas jet spatial density distribution. Each measurement of gas jet density can be divided into three parts:

- recording of individual interferograms of the gas jets,
- phase retrieval by a wavelet transform algorithm,
- density reconstruction by tomographic algorithms or by Abel transform method.

For each measurement, we record two interferograms – a signal interferogram with the gas jet and a background interferogram without the gas jet, and we subsequently subtract the background one from the signal one. This allows us to minimize the noise and the systematic errors, e.g. alleviate the effect of the imperfections in the optical system elements. The phase is retrieved by a 2D Continuous Wavelet Transform (CWT) and a direct Maximum ridge detection algorithm. CWT allows to be tuned to each application case by choice of optimal wavelet function for the phase retrieval. The density reconstruction is done by either tomographic methods from multiple projections of the jet for complex gas distributions or by Abel transform from single projections for rotationally symmetric gas jets. Here, we use the Filtered-back projection method with a Hann filter [20]-[21] for the density characterization of a slit nozzle. We perform 18 projections of the jet with a step of 10 degrees between them.

2.2 Gas nozzles for LPA experiments

The gas jets are essential targets for LPA experiments as they offer the possibility to design different gas density distribution for the focused laser pulse. In particular, the gas jets that are employed as LPA targets include rotationally symmetric gas jet produced by cylindrical nozzles, non-rotationally symmetric jets generated by slit nozzles of various dimensions, jets with tailored shock fronts generated by blades or wires obstructing the gas flow [17], [22]-[25]. The diversity of gas jets results from the significant effect that the gas density spatial distribution has on laser-plasma interaction, e.g. it has been demonstrated that a plasma density longitudinal down-ramp can improve the stability of the generated electron beam [26]-[27]. Thus, the precise knowledge of gas density distribution is essential for the performance of the laser-plasma accelerators.

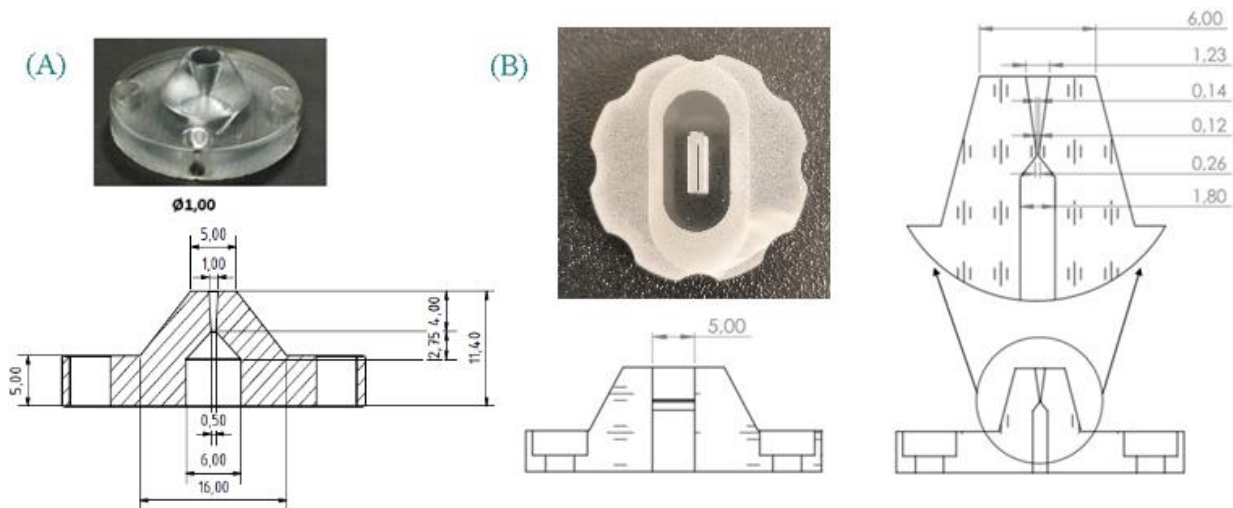


Figure 2. Sketches and images of the nozzles used as LPA targets – (A) cylindrical nozzle with de Laval shape and (B) slit nozzle 5 mm × 1 mm with de Laval shape along the long side.

Here, two different types of gas jets are characterized – a rotationally symmetric gas jet produced by a cylindrical nozzle with de Laval shape, shown in Figure 2 (A) and an elongated jet produced by a $5 \text{ mm} \times 1 \text{ mm}$ slit nozzle with de Laval shape along the long side and straight walls along the short side as shown in Figure 2 (B). The slit nozzle was fabricated from fused silica via the bottom-up milling approach using nanosecond laser [28],[29]. This technique allowed the precise 2.5D processing with high material removal rate reaching $0.07 \text{ mm}^3/\text{s}$ for the inner converging-diverging channel with only a 1.7 W average laser power. The average peak-to-valley distance of the milled surface does not exceed $10 \text{ }\mu\text{m}$ using this technique [30].

The two jets are characterized by the proposed double-pass interferometer and also with the standard single-pass interferometer configuration. This comparison allows us to validate the performance of the double-pass interferometer and quantify its capabilities.

The gas nozzle is set on top of a rotation stage and two linear stages. The rotation stage provides the capability to turn the holder by a precise angle and to record multiple projections at these angles, This is required for the tomographic measurements. The two orthogonal translation stages allow for the precise alignment of the rotation axis of the rotation stage axis to the required position of the nozzles. The jets are operated in a pulsed regime using a pulsed valve synchronized with a delay generator with an opening time of the valves of 10 ms.

3. TOMOGRAPHIC CHARACTERIZATION OF GAS JETS

3.1 Comparison of single-pass and double-pass probing

In order to verify the capabilities of the proposed double-pass configuration, we have characterized the rotationally symmetric gas jet, produced by a cylindrical nozzle (see Figure 2 (A)) and the non-rotationally elongated gas jet, produced by a slit nozzle (see Figure 2(B)) with both the single-pass and double-pass configurations and compare the obtained results.

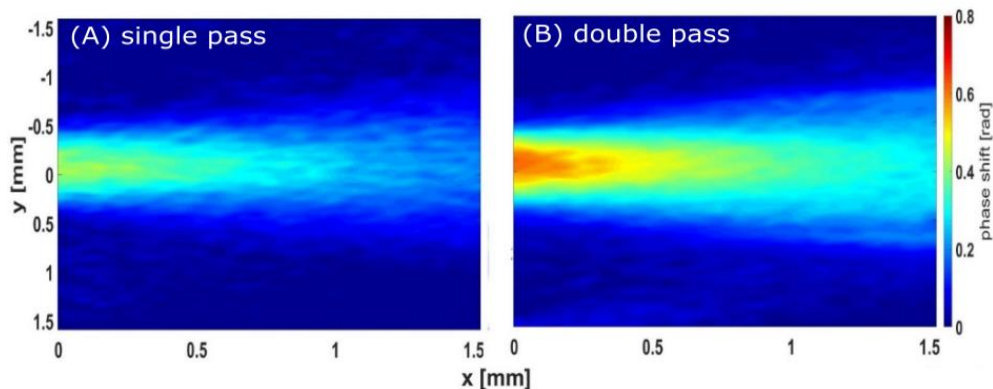


Figure 3. Phase maps comparison of a rotationally symmetric Ar gas jet measured by single (A) and double (B) pass interferometric configurations with valve backing pressure of 1.6 bar.

The gas jet phase map from the interferometric measurements of the symmetric gas jet obtained at the 1.6 bar of Ar is shown in Figure 3. We can see in Figures 3 (A) and 3 (B) that the double-pass configuration results in a two-fold increase in the phase acquired by the probe laser beam – maximum phase for double-pass is 0.88 rad, and maximum phase for single-pass is 0.44 rad. To quantify the sensitivity of the double-pass configuration in addition to the phase values, we also need the background noise value. We estimate it for both double and single-pass measurements as a standard deviation of the phase shift in a square area of $1 \text{ mm} \times 1 \text{ mm}$ on the side of the interferograms where no gas density is expected. The background noise values estimated this way are 0.02 rad for both configurations. These results show that the double-pass configuration provides two times higher sensitivity than the standard single pass. This result is extremely important for the trend in LPA experiments of minimizing the gas jet dimensions and decreasing the gas jet densities, especially for low refractive index gas like helium, as the increased sensitivity can be vital for characterizing the gas interaction medium and its specific features.

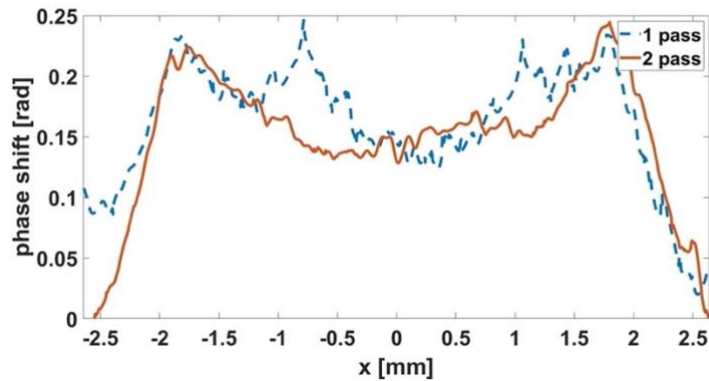


Figure 4. Phase profile comparison of a non-rotationally symmetric elongated gas jet, produced by a slit nozzle, measured by single and double pass interferometric configurations performed at 20 bar of Ar (measured before the valve) along the long side of the nozzle at the height of 1 mm above the nozzle edge.

The comparison of phase profiles of the non-rotationally symmetric gas jet from a slit nozzle obtained with double-pass and single-pass setups is shown in Figure 4. The phase profiles obtained at 1 mm above the nozzle at 20 bar backing pressure of Ar (pressure measured before the valve) along the long side (5 mm) of the nozzle are shown. It is seen in the figure that the phase profiles have a characteristic shape with two density peaks near the walls and a lower plateau in the middle. The phase profile comparison shows clearly that the double-pass configuration has lower noise, which allows for better accuracy of the profile characterization.

3.2 Tomographic reconstruction of non-rotationally symmetric gas jets generated by a slit nozzle

We apply the double-pass configuration for density characterization of the slit 5 mm × 1 mm nozzle used for LPA experiments at 20 bar Ar. Here, we used 18 projections of the gas jet each taken at a step of 10 degrees apart.

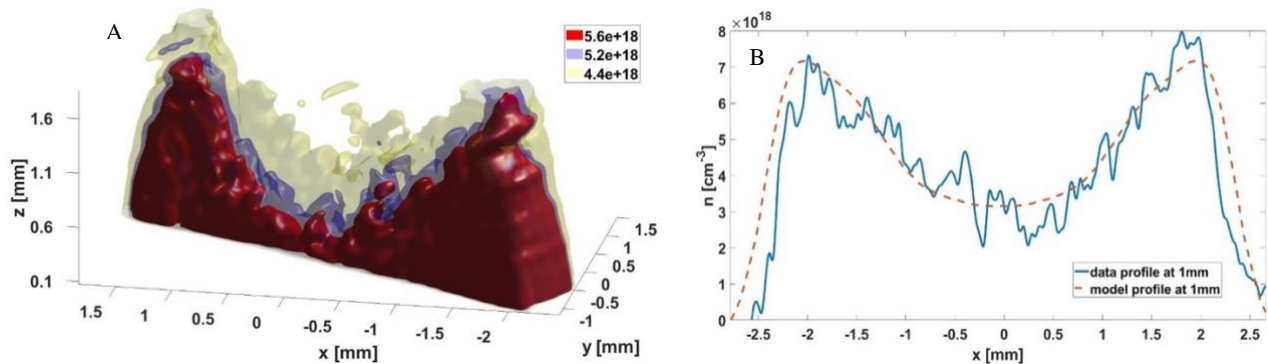


Figure 5. Tomographic density reconstruction of a slit nozzle gas jet at 20 bar Ar for LPA applications: (A) tomography density reconstruction; (B) density profiles of interferometric measurements with double-pass configuration and of fluid simulations at the height of 1 mm above the nozzle.

The results from the tomographic reconstruction are shown in Figure 5. In the figure, we can see the 3D density map of the slit nozzle represented by iso-surfaces of equal gas density with different colors. It is seen in the figure that there are three separated density regions – two side density peaks and a lower central plateau and the ratio between the two regions is two-fold. The density ratio between the peak and the plateau is a function of the nozzle dimensions and the throat orifice size, which allows for obtaining different peak-plateau ratios with modification of the nozzle dimensions. The measured values are in good agreement with the simulation results in both the side peaks and the central plateau region, as shown in Figure 4. The noise visible in tomographic density plot can be further diminished by increasing the number of projections recorded for the reconstruction.

In Figure 5 (B), a comparison is made between density plots from the tomographic density reconstructions and 3D gas density fluid simulations (for more information on the simulations see [31]). It is seen that there is a good agreement between the measurement and the simulation in both the side peaks and the central plateau region.

In LPA experiments, the slit nozzle with the density profile as shown in Figure 5 can be utilized for different purposes: the transverse profile can be used for limiting the acceleration length and thus controlling/limiting the electron beam energy; the longitudinal profile can be used for multi-stage acceleration taking advantage of the three separate density regions, first density ramp to inject the electron bunch, low-density plateau to boost the acceleration and the second ramp to enhance the X-ray generation.

4. CONCLUSIONS AND PERSPECTIVES

We report on a new optical probing technique – a double-pass interferometer with Wollaston prism that is suitable for density characterization of LPA gas jet targets with increased sensitivity and with multiple projections enabling tomographic reconstruction. This technique is employed to characterise rotationally symmetric gas jets and tailored gas jets used as gas targets for LPA experiments. It was demonstrated that the double-pass technique exhibits a two-fold increase in the sensitivity compared to the standard single-pass configuration. The tomographic reconstruction of the tailored gas jet produced by a slit nozzle shows that the technique is able to describe the complex gas density spatial distribution. In the future, the technique can be upgraded to a higher number of passes by polarization switching of the probing laser beam [32] and can also be applied in reflectance or absorption configurations.

Acknowledgments: This research was supported by the project Advanced research (ADONIS) (CZ.02.1.01/0.0/0.0/16_019/0000789) and by the project High Field Initiative (HiFI) (CZ.02.1.01/0.0/0.0/15_003/0000449), both from European Regional Development Fund. The results of Project LQ1606 were obtained with the financial support of the Ministry of Education, Youth, and Sports as part of targeted support from the National Programme of Sustainability II.

REFERENCES

- [1] Tajima, T. and Dawson, J. M., "Laser electron accelerator", *Phys. Rev. Lett.*, **43**, 267-270 (1979).
- [2] Rousselet al., "Production of a keV X-Ray Beam from Synchrotron Radiation in Relativistic Laser-Plasma Interaction", *Phys. Rev. Lett.*, **93**, 1-4 (2004).
- [3] Albert, F., et al. "Betatron x-ray radiation in the self-modulated laser wakefield acceleration regime: Prospects for a novel probe at large scale laser facilities" *Nuclear Fusion* **59.3** 032003 (2018).
- [4] Chaulagain, U., et al. "LWFA-Driven Betatron Source for Plasma Physics Platform at ELI Beamlines." *International Conference on X-ray Lasers*. Springer, Cham, 2018.
- [5] Nejdil, J., et al. "Progress on laser-driven x-ray sources at ELI Beamlines." *X-Ray Lasers and Coherent X-Ray Sources: Development and Applications XIII*. Vol. 11111. International Society for Optics and Photonics, 2019.
- [6] Kozlova, M., et al. "Laser-driven plasma-based incoherent x-ray sources at PALS and ELI beamlines." *International Conference on X-ray Lasers*. Springer, Cham, 2016.
- [7] Jourdain, N., et al., "The L4n laser beamline of the P3-installation: Towards high-repetition rate high-energy density physics at ELI-Beamlines" *Matter and Radiation at Extremes* **6.1** 015401(2021).
- [8] Chaulagain, U. et al., "ELI Gammatron Beamline: Dawn of ultrafast hard X-ray science" (to be published) <https://www.eli-beams.eu/facility/experimental-halls/e2-x-ray-sources/betatron-compton-beamline/>
- [9] Döpp, A., et al. "Quick x-ray microtomography using a laser-driven betatron source." *Optica* **5.2** 199-203 (2018).
- [10] Chaulagain, U., et al., "X-ray phase contrast imaging of biological samples using a betatron x-ray source generated in a laser wakefield accelerator" *Proc. SPIE*, **10240**, 1024014 (2017).
- [11] Wood, J.C., et al. "Ultrafast imaging of laser driven shock waves using betatron x-rays from a laser wakefield accelerator." *Scientific reports* **8.1** (2018): 1-10.
- [12] Mahieu, B., et al., "Probing warm dense matter using femtosecond x-ray absorption spectroscopy with a laser-produced betatron source" *Nat. commun.* **9**, 1-6 (2018).
- [13] Huang, K., et al. "Simultaneous generation of quasi-monoenergetic electron and betatron X-rays from nitrogen gas via ionization injection." *Appl. Phys. Lett* **105.20** 204101 (2014):.

- [14] Boháček, K., et al. "Stable electron beams from laser wakefield acceleration with few-terawatt driver using a supersonic air jet." *Nuclear Instruments and Methods in Physics Research Section A: Accelerators, Spectrometers, Detectors and Associated Equipment* **883** 24-28 (2018).
- [15] Chen, L. M., et al. "Bright betatron X-ray radiation from a laser-driven-clustering gas target." *Scientific reports* **3.1** 1-5 (2013).
- [16] Bohacek, K., et al. "Laser-driven electron beam generation for secondary photon sources with few terawatt laser pulses." *Laser Acceleration of Electrons, Protons, and Ions IV*. Vol. 10240. International Society for Optics and Photonics, 2017.
- [17] Kozlová, M. et al., "Hard X Rays from Laser-Wakefield Accelerators in Density Tailored Plasmas," *Phys. Rev. X* **10** 011061, 1-7 (2020).
- [18] Fourmaux, S. et al., "Laser-based synchrotron X-ray radiation experimental scaling." *Opt. Express* **28**, 3147-3158, (2020)
- [19] Nejd, J., et al., "Imaging Michelson interferometer for a low-density gas jet characterization" *RSI* **90**, 065107 (2019).
- [20] Kak A. C. and Slaney M., "Principles of computerized tomographic imaging" IEEE Press, 203-274 (1999).
- [21] Radon J., "On the determination of functions from their integral values along certain manifolds," *IEEE transactions on medical imaging* **5**, 170-176 (1986).
- [22] Geddes C. G. R., et al., "Plasma-Density-Gradient Injection of Low Absolute-Momentum-Spread Electron Bunches," *Phys. Rev. Lett.* **100** 215004, 1-4 (2008).
- [23] Bulanov S. et al., "Particle injection into the wave acceleration phase due to nonlinear wake wave breaking," *Phys. Rev. E* **58**, R5257-R5260 (1998).
- [24] Schmid K., et al., "Density-transition based electron injector for laser driven wakefield accelerators," *Phys. Rev. ST Accel. Beams* **13** 091301, 1-5 (2010).
- [25] He Z.-H., et al., "High repetition-rate wakefield electron source generated by few-millijoule, 30 fs laser pulses on a density downramp" *New J. Phys.* **15**, 1-11 (2013).
- [26] Gonsalves, A. J., et al., "Tunable laser plasma accelerator based on longitudinal density tailoring," *Nat. Phys.* **7**, 862–866 (2011).
- [27] Thaury, C., et al., "Shock assisted ionization injection in laser-plasma accelerators," *Sci. Rep.* **5**, 16310 (2015)
- [28] Gečys, P., et al., "Nanosecond Laser Processing of Soda-Lime Glass," *J. Laser Micro/Nanoengineering* **10**(3), 254–258 (2015).
- [29] Tomkus, V., et al., "High-density gas capillary nozzles manufactured by hybrid 3D laser machining technique from fused silica," *Opt. Express* **26**(21), 27965 (2018).
- [30] Tomkus, V., et al., "Impact of the wall roughness on the quality of micrometric nozzles manufactured from fused silica by different laser processing techniques," *Appl. Surf. Sci.* **483**(October 2018), 205–211 (2019).
- [31] Lorenz S., et al., "Characterization of supersonic and subsonic gas targets for laser wakefield electron acceleration experiments," *Matter and Radiation at Extremes* **4** 015401, 1-6 (2019).
- [32] Karatodorov, S., et al., Multi-pass probing for high-sensitivity tomographic interferometry (submitted)
- [33] D. Bleiner, *The Science and Technology of X-ray Lasers: A 2020 Update Proc. SPIE 11886*, 1188602 (2021)